BIOCHEMICAL PHARMACOLOGY 75 (2008) 383–394

available at www.sciencedirect.com

ScienceDirect

journal homepage: www.elsevier.com/locate/biochempharm

KRIBB3, a novel microtubule inhibitor, induces mitotic arrest and apoptosis in human cancer cells

Ki Deok Shin [a,c], *Young Ju Yoon* [a], *Yeong-Rim Kang* [a], *Kwang-Hee Son* [a], *Hwan Mook Kim* [b], *Byoung-Mog Kwon* [a,*], *Dong Cho Han* [a,*]

[a] *Molecular Cancer Research Center, Korea Research Institute of Bioscience and Biotechnology, 52 Eoeun-dong Yuseong-gu, Daejeon 305-806, Republic of Korea*

[b] *Bio-Evaluation Center, Korea Research Institute of Bioscience and Biotechnology, 52 Eoeun-dong Yuseong-gu, Daejeon 305-806, Republic of Korea*

[c] *Department of Biochemistry, Yonsei University, Seoul 120-749, Republic of Korea*

ARTICLE INFO

Article history:
Received 20 July 2007
Accepted 22 August 2007

Keywords:
Isoxazole
Microtubule inhibitor
Mitotic arrest
Apoptosis
Bax activation
Cancer therapy

ABSTRACT

KRIBB3 (5-(5-ethyl-2-hydroxy-4-methoxyphenyl)-4-(4-methoxyphenyl) isoxazole) inhibited cancer cell growth *in vitro* and *in vivo*. Flow cytometry studies showed that KRIBB3 caused cell cycle arrest at the G_2/M phase and subsequent apoptosis. This was confirmed as accumulation of Cyclin B1 and cleavage of poly(ADP-ribose) polymerase (PARP) were detected. While transient inhibition by KRIBB3 led to reversible mitotic arrest, prolonged exposure to KRIBB3-induced apoptosis. Co-immunoprecipitation experiments showed that KRIBB3 initially induced association of inhibitory Mad2 with p55CDC (mammalian homologue of CDC20), an activator of APC/C (anaphase-promoting complex/cyclosome), suggesting that the mitotic spindle checkpoint was activated by KRIBB3. However, the level of this inhibitory complex of Mad2 with p55CDC was gradually decreased 24 h after KRIBB3 treatment, and was hardly detectable after 48 h, indicating some slipping of the mitotic checkpoint. Consistent with these observations, KRIBB3 activated the mitotic spindle checkpoint by disrupting the microtubule cytoskeleton. KRIBB3 was proven to be a tubulin inhibitor using *in vitro* polymerization assays and *in vivo* indirect immunofluorescence staining. The temporal pattern of Bax activation by KRIBB3 was similar to PARP cleavage, suggesting that Bax is a mediator of KRIBB3-dependent apoptosis. Furthermore, when KRIBB3 was administered intraperitoneally into nude mice at 50 mg/kg or 100 mg/kg, it inhibited 49.5 or 70.3% of tumor growth, respectively. These results suggest that KRIBB3 is a good drug candidate for cancer therapy.

1. Introduction

Chemicals that interfere with cell cycle progress have attracted much attention in cancer research because they can inhibit the proliferation of cancer cells. Among various anticancer drug targets known to date, those targeting microtubules are some of the most successful cancer therapeutics [1]. Traditional anti-microtubule drugs produce "unattached" kinetochores in mitosis by altering microtubule dynamics, and cause long-term mitotic arrest [2,3].

The mitotic spindle checkpoint is the major cell cycle control mechanism in mitosis (for review, see Refs. [2,4,5]). In order to recognize and interact with mitotic substrates, APC/C requires the specific factor CDC20 (cell-division-cycle 20

* *Corresponding authors.*
E-mail addresses: kwonbm@kribb.re.kr (B.-M. Kwon), dchan@kribb.re.kr (D.C. Han).
0006-2952/$ – see front matter
doi:10.1016/j.bcp.2007.08.027

homologue). Genetic and biochemical studies have suggested that the most downstream event in checkpoint regulation is the inhibition of CDC20. The signal generators of the mitotic checkpoint are "unattached kinetochores" which recruit mitotic checkpoint components and convert these into an inhibitory complex, which is composed of Mad2 (mitotic arrest deficient 2), BubR1 (a hybrid of Mad3 and Bub1), Bub3 (budding uninhibited by benzimidazole 3), and CDC20 [6,7]. Inhibitory Mad2 and/or BubR1 tightly associate with CDC20 and prevent it from activating APC/C, blocking degradation of Cyclin B1.

Drug-mediated mitotic-checkpoint-dependent-arrest is often followed by cell death [2]. Although the capacity to undergo apoptosis is inherent to all cells, their susceptibility varies markedly and is influenced by external and internal events [8]. Members of the Bcl-2 family of proteins play crucial roles in the regulation of apoptosis through controlling mitochondrial function and releasing proapoptotic proteins from the mitochondria. Because mitochondria interact with microtubules, it is likely that mitochondria may connect microtubule damage to the apoptotic machinery, acting as appropriate, and timing switches for the onset of apoptosis. Bcl-2 overexpression suppresses the apoptotic response induced by distinct microtubule-active drugs without affecting their actions on microtubules or on cell cycle arrest at G_2/M [9,10]. Bim (Bcl-2 interacting mediator of cell death) [11] and Bmf (Bcl-2 modifying factor) [12] are important linkers of cytoskeleton and apoptotic machinery since they are indirectly sequestered by the microtubule (Bim) or actin (Bmf) cytoskeleton. Apoptotic stimuli lead to the release of Bim from microtubules, and Bim is therefore free to translocate to the mitochondria, where it binds Bcl-2 and Bcl-X_L to promote apoptosis through neutralization of the antiapoptotic activity of Bcl-2 and Bcl-X_L by forming Bim/Bcl-2 or Bim/Bcl-X_L heterodimers [11], or through additional mechanisms, including Bax activation [13].

Vinca alkaloids inhibiting microtubule polymerization, have been used in the treatment of cancer over 30 years [14]. Unlike vinca alkaloids, taxanes promote tubulin polymerization, stabilize microtubules, and thereby inhibit microtubule dynamics, causing abnormal mitotic spindle and mitotic arrest [15,16]. Although the vinca alkaloids and the taxanes are both effective in the treatment of cancer, their potential is limited by the appearance of drug-resistant cancer cells during cancer treatment [17]. One mechanism leading to drug resistance is mediated by overexpression of efflux pumps, specifically the p-gp170 [18] and MRP pumps [19]. These efflux pumps are able to reduce the intracellular concentration of taxanes or vinca alkaloids to a less toxic level.

KRIBB3 was reported to inhibit tumor cell migration and invasion at doses of 0.1–1 μM [20]. However, it inhibited proliferation of MDA-MB-231 with a GI_{50} of >25 μM, where GI_{50} is the concentration at which 50% inhibition of cell growth is seen. This indicates that KRIBB3 significantly inhibits cell migration without cytotoxicity. Using affinity chromatography, Hsp27 was identified as a molecular target of KRIBB3. Several other studies point to the ability of Hsp27 to increase the metastatic potential of tumor cells in nude mice, as well as to enhance their resistance to therapy [21,22]. Higher levels of Hsp27 expression are commonly detected in a variety of different cancers including breast [23,24], prostate [25], gastric [26], and ovarian [27,28] cancer.

Here, we report the biological properties of KRIBB3, which displays strong antimitotic activity against cancer cells. KRIBB3 exerts its antiproliferative activity through inhibition of tubulin polymerization and by activating the mitotic spindle checkpoint. In addition, KRIBB3 is not a substrate of p-gp170, and it retains its activity in cell lines with MDR. When KRIBB3 was administered to nude mice, tumor growth was significantly inhibited compared to control mice, supporting its anticancer activity *in vivo*.

2. Materials and methods

2.1. Reagents and antibodies

Rabbit polyclonal anti-phospho-Histone H3 (Ser 10) antibody was purchased from Upstate Biotechnology. Antibodies against Hsp27 and PARP were purchased from Cell Signaling. Antibodies against Bax, Mad2, and BubR1 were purchased from BD biosciences (San Jose, CA). Antibodies for Cyclin B1, p55CDC, and actin were purchased from Santa Cruz Biotechnology, Inc. (Santa Cruz, CA). Monoclonal anti-Bax 6A7 antibody was purchased from Sigma (St. Louis, MO). Monoclonal anti-α-tubulin was purchased from Molecular Probes. Chemicals used in these experiments were purchased from Sigma Chemical (St. Louis, MO) and Calbiochem (San Diego, CA). KRIBB2 (4-ethyl-5-methoxy-2(3-methyl-4-phenylisoxazole-5-yl)phenol) and KRIBB3 (5-(5-ethyl-2-hydroxy-4-methoxyphenyl)-4-(4-methoxyphenyl) isoxazole) were synthesized in our laboratory.

2.2. Cell culture, cell proliferation assays, Western blotting, and immunoprecipitation

The cancer cell lines were originally obtained from ATCC. HCT-116 (human colon cancer cell line), HCA-7 (human breast cancer cell line), and SK-OV-3 cells (human ovarian cancer cell line) were maintained in McCoy's 5A (Invitrogen) medium supplemented with penicillin (50 units/ml) and streptomycin (50 μg/ml). MDA-MB-231 (human breast cancer cell line), HT-29, HCT-15, SW620 (human colon cancer cell line), NCI-H23 (human non-small lung cancer cell line), DU-145, and PC-3 cells (human prostate cancer cell line) were maintained in RPMI 1640 (Gibco/BRL). A549 (human non-small lung cancer cell line) and HeLa cells (human cervical adenocarcinoma cell line) were maintained in Dulbecco's modified Eagle medium (Gibco/BRL). All culture media were supplemented with 10% heat-inactivated fetal bovine serum (Gibco/BRL). Cell cultures were maintained at 37 °C under a humidified atmosphere of 5% CO_2 in an incubator. A proliferation assay was performed as previously described [20]. Briefly, 6000 cells were seeded into 96-well plates in media containing 10% FBS. After 20–24 h, cells were replenished with fresh complete medium containing either a test compound or 0.1% Me_2SO. After incubation for 48 h, the cell proliferation reagent WST-1 (Roche Applied Science) was added to each well. The amount of WST-1 formazan produced was measured at 450 nm using an ELISA Reader (Bio-Rad, CA). Western blotting and immunoprecipitation were then performed as previously described [29].

2.3. Cell synchronization and cell cycle analysis

For synchronization at metaphase, cells were treated with nocodazole (1 μM) at 37 °C for 15 h. After treatment, metaphase cells were collected by the gentle shake-off method, centrifuged at 300 × *g* for 5 min at room temperature, and washed twice with fresh medium. To relieve cells from the mitotic phase arrest, cells were replated in a 100 mm cell culture dish (1×10^6 cells/dish) and incubated at 37 °C in fresh medium for various time periods. To analyze the DNA content by flow cytometry, cells were trypsinized, washed twice with phosphate-buffered saline and fixed with 3 ml of ice-cold 70% ethanol overnight. Fixed cells were washed twice with PBS containing 1% fetal bovine serum. The collected cells were resuspended in PBS (100 μl/1×10^5 cells) and treated with 100 μg/ml of RNase A at 37 °C for 30 min. Propidium iodide (PI) was then added at a final concentration of 50 μg/ml for DNA staining, and 20,000 fixed cells were analyzed on a FACScalibur (Becton Dickinson, San Jose, CA). Cell cycle distribution was analyzed using the Modifit program (Becton Dickinson).

2.4. Tubulin polymerization assay

For the detection of polymerization of tubulin/microtubules, CytoDYNAMIX Screen 01 kits were purchased form Cytoskeleton, Inc. (Denver, CO). Tubulin proteins (>97% purity) were suspended (300 μg/sample) with 100 μl of G-PEM buffer (80 mM PIPES, 2 mg $MgCl_2$, 0.5 mM EGTA, 1.0 mM GTP, pH 6.9) plus 5% glycerol in 0.1% DMSO at 4 °C, with and without test compound. Next, the sample mixture was transferred to the prewarmed 96-well plate, and polymerization of tubulin was measured by the change in absorbance at 340 nm every 1 min for 70 min (Wallac victor2; Perkin-Elmer, Inc., Wellesley, MA) at 37 °C.

2.5. Immunofluorescence microscopy

HCT-116 cells were plated on an 18 mm coverslip coated with 50 mg/ml of Poly-L-Lysine. Cells were incubated in a 37 °C incubator to allow cells to attach and spread. At the end of incubation, the cells were fixed with 3% formaldehyde for 10 min, washed three times with PBS for 5 min each time, permeabilized with 0.5% Triton X-100 for 5 min, washed three times, and stained with primary antibodies (α-tubulin (1:50)) for 1 h at room temperature. After washing three times with PBS, the bound mouse IgG was detected with Texas Red-conjugated anti-mouse antibody (1:100) and counterstained with 1 μg/ml of DAPI (4′, 6-diamidino-2-phenylindole) in PBS for 1 h at room temperature. Images of stained cells were examined under a Zeiss LSM 510 META confocal microscope (Carl Zeiss, Inc., Thornwood, NY).

2.6. Detection of Bax conformational change (activation)

Metaphase synchronized cells were treated with 0.1% DMSO or 1 μM of KRIBB3. The method was modified from the previous description [31]. Briefly, cells were collected and lysed with Chaps lysis buffer (10 mM Hepes (pH 7.4), 150 mM NaCl, and 1% Chaps). Cell lysates containing 500 μg protein were incubated with the anti-Bax 6A7 monoclonal antibody for 3 h at 4 °C in a rotary shaker, after which 40 μl of protein G-agarose beads were added. After 2 h, lysates containing beads were centrifuged and washed three times with Chaps lysis buffer. Bead-bound proteins were resolved by SDS-PAGE and immunoblotted using an anti-Bax monoclonal antibody (BD bioscience).

2.7. Knockdown of Hsp27 protein using Hsp27 siRNA

The human Hsp27 small interfering RNA (siRNA) duplex (5′-GUCUCAUCGGAUUUUGCAGC-3′) was purchased from Bioneer, Inc. (Daejeon, KOREA). A Silencer Negative Control #1 siRNA was purchased from Ambion, Inc. (Austin, TX) as a control. Cells plated at a density of 8×10^4 cells per well in six-well plates were transfected with 50 nM or 100 nM of Hsp27 specific and control siRNA oligoduplexes after preincubation for 20 min with Oligofectamine in serum-free OPTI-MEM (Invitrogen). Four hours after transfection, RPMI 1640 media containing 30% serum (without antibiotics) was added, yielding a final concentration of 10% serum. Forty-eight hour after transfection, cells were harvested for cell cycle analysis or for preparation of whole cell lysates.

2.8. Nude mouse xenograft assay

Seven-week-old female inbred specific-pathogen-free (SPF) BALB/c nude mice were obtained from the Charles River Co. (Japan), and were housed in sterile conditions under 12 h light:12 hdark cycles, and fed food and water *ad libitum*. For the evaluation of the *in vivo* anti-tumor activity of KRIBB3, HCT-116 cells (0.3 ml of 3×10^6 cells/ml) were implanted subcutaneously into the right flank of the mice on day 0. KRIBB3 or doxorubicin was dissolved in 0.5% Tween 80 and administered intraperitoneally daily for 16 days at a concentration of 50 or 100 mg/kg for KRIBB3 or 2 mg/kg for doxorubicin. The dosage amount was 0.2 ml per 20 g body weight. Tumor volumes were estimated as length (mm) × width (mm) × height (mm)/2. To determine the toxicity of the compound, the body weight of tumor-bearing animals was measured. On day 16, the mice were sacrificed and the tumors were removed and weighed.

3. Results

3.1. Inhibition of tumor cell growth by KRIBB3

To determine the effect of isoxazoles on the growth of cancer cells, HCT-116 colon cancer cells were treated with compounds at different concentrations (0–100 μM) for 48 h (Fig. 1A). KRIBB2 is an inactive structural analogue of KRIBB3. KRIBB3 exhibited a dose-dependent inhibition of cell growth in a broad range of concentrations, and the GI_{50} value of KRIBB3 for *in vitro* growth inhibition was approximately 0.35 μM, where GI_{50} is the inhibitor concentration at which 50% inhibition of cell growth is seen.

Failure in cancer chemotherapy is often related to multidrug resistance (MDR). Therefore, we tested whether MDR1 overexpression confers resistance to KRIBB3. Paclitaxel and vinblastin are the most widely used antimitotic cancer drugs, and are substrates of P-glycoprotein (MDR1). Therefore, we

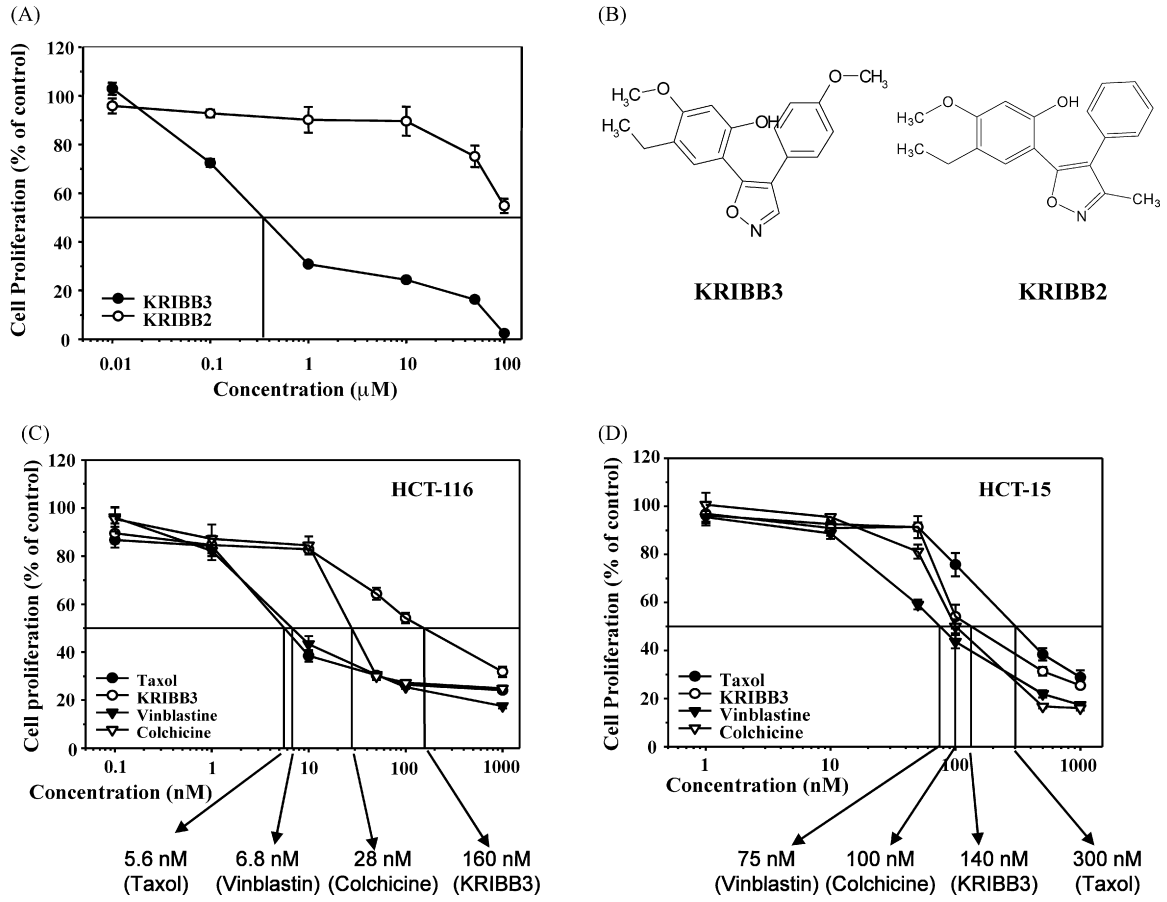

Fig. 1 – Structure and activity of isoxazole compounds, paclitaxel, vinblastin, and colchicine on the proliferation of HCT-116 or HCT-15 tumor cells. HCT-116 or HCT-15 cells were treated with different concentrations of compounds or with vehicle solvent (0.1% DMSO), and their viability was determined using the WST-1 assay 48 h after treatment. The results were expressed relative to the vehicle-treated cells. This data is from one out of three independent experiments with similar results.

used these chemicals as positive compounds for MDR1. HCT-15 is an MDR1 overexpressing colorectal carcinoma. As expected, HCT-15 has profound resistance to paclitaxel (53-fold), vinblastin (11-fold), and colchicines (4-fold) compared with HCT-116. In contrast, KRIBB3 is equally potent toward HCT-116 and HCT-15 (Fig. 1C and D), suggesting that KRIBB3 can be effective against MDR1-overexpressing drug-resistant cells.

Similarly, the effect of KRIBB3 on the proliferation of various tumor cell lines was analyzed (Table 1). Because more than 50% of human cancers have mutated p53, which is known to be an important regulator of cell cycle progression and apoptosis, we chose to study both p53 wild type and p53-deficient cancer cell lines. Fortunately, KRIBB3 was able to exert its inhibitory activity in a p53-independent pathway, as shown by its similar effects on the p53 expressing and deficient cell lines.

3.2. *Inhibition of Hsp27 does not block tumor cell growth*

Previously, we reported that KRIBB3 inhibited tumor cell migration by blocking PKC-dependent phosphorylation of Hsp27 through direct binding to Hsp27 [20]. To determine whether inhibition of Hsp27 affects cell proliferation, we introduced Hsp27 siRNA into HCT-116 cells. As shown in Fig. 2A, expression of Hsp27 was largely eliminated from HCT-116 cells after transfection of Hsp27 siRNA, indicating that the siRNA can target Hsp27 mRNA efficiently in HCT-116 cells. Next, we analyzed the proliferation of HCT-116 cells after the cells were treated with control siRNA, Hsp27 siRNA, or H_2O. Surprisingly, there was no detectable inhibition of proliferation by Hsp27 siRNA transfection (Fig. 2B). This result implies that KRIBB3 inhibits the proliferation of HCT-116 cells in a Hsp27-independent manner. In addition, knockdown of Hsp27 using siRNA did not affect the HCT-116 cell cycle (Fig. 2C).

3.3. *KRIBB3 arrests cells in the G_2/M phase*

Because KRIBB3 inhibited cancer cell growth, we analyzed the effect of KRIBB3 on the cell cycle profile. HCT-116 cells were treated with 1 μM KRIBB3 and harvested at 0, 1, 3, 6, 12, 24, and 48 h after treatment, and then analyzed with a FACScalibur. When HCT-116 cells were treated with KRIBB3, an increase in the proportion of G_2/M phase cells could be detected (Fig. 3A

Table 1 – Inhibitory effect of KRIBB3 on the proliferation of human tumor cells

Tumor cell line	p53	GI_{50} (μM)
HCT-116	Wild-type	0.35
HCT-15	Deficient	0.3
SW620	Deficient	0.8
HT-29	Deficient	23
HCA-7	Deficient	0.38
MDA-MB-231	Deficient	25
NCI-H23	Wild-type	0.64
A549	Wild-type	1.2
DU-145	Deficient	0.28
PC-3	Deficient	0.48
SK-OV-3	Deficient	0.6
HeLa	Wild-type	0.75

Cells were treated with different concentrations of KRIBB3 or vehicle solvent (0.1% DMSO), and proliferation was determined using WST-1 at 48 h after the treatment. This data is from one of two independent experiments with similar results.

and B). Seventy percent of cells were arrested at the G_2/M phase checkpoint 12 h after treatment. Because KRIBB3 arrested the cell cycle in the G_2/M phase, we used the well-known antimitotic compound nocodazole as a control for further study. Treatment with nocodazole showed a similar effect on the cell cycle profile of HCT-116 cells. In addition, when DU-145 cells were treated with KRIBB3, cell cycle arrest could be detected at the G_2/M phase (data not shown). Interestingly, treatment of asynchronous HCT-116 cells with KRIBB3 resulted in the accumulation of cells with a hyperploid DNA content (>4 N) (Fig. 3C). Thirty-seven percent of cells became hyperploid (>4 N) 48 h after KRIBB3 treatment. Similarly, 36% of nocodazole-treated cells were hyperploid. This result suggests that KRIBB3 first arrested cell cycle and then underwent mitosis to become hyperploid.

Cell cycle arrest in the G_2/M phase was confirmed by detecting G_2/M phase-specific accumulation of Cyclin B1 and phosphorylation of Histone H3 (Ser10) (Fig. 3D). The Cyclin B1 protein levels increased after KRIBB3 treatment and remained elevated for 48 h. Similarly, phosphorylation of Histone H3 (Ser 10) increased after KRIBB3 treatment and remained elevated for 24 h. However, phosphorylation of Histone H3 (Ser 10) decreased to its basal level after 48 h. The temporal patterns of Cyclin B1 accumulation and Histone H3 phosphorylation are consistent with cell cycle arrest at the G_2/M phase as shown in Fig. 3.

In order to determine whether KRIBB3-treated cells were blocked at the G_2 phase or at the mitotic phase, cells were analyzed for progression from mitotic arrest. To synchronize cells in mitosis, HCT-116 cells were treated with 1 μM nocodazole for 15 h. After collection, synchronized mitotic cells were replated in medium containing DMSO or KRIBB3.

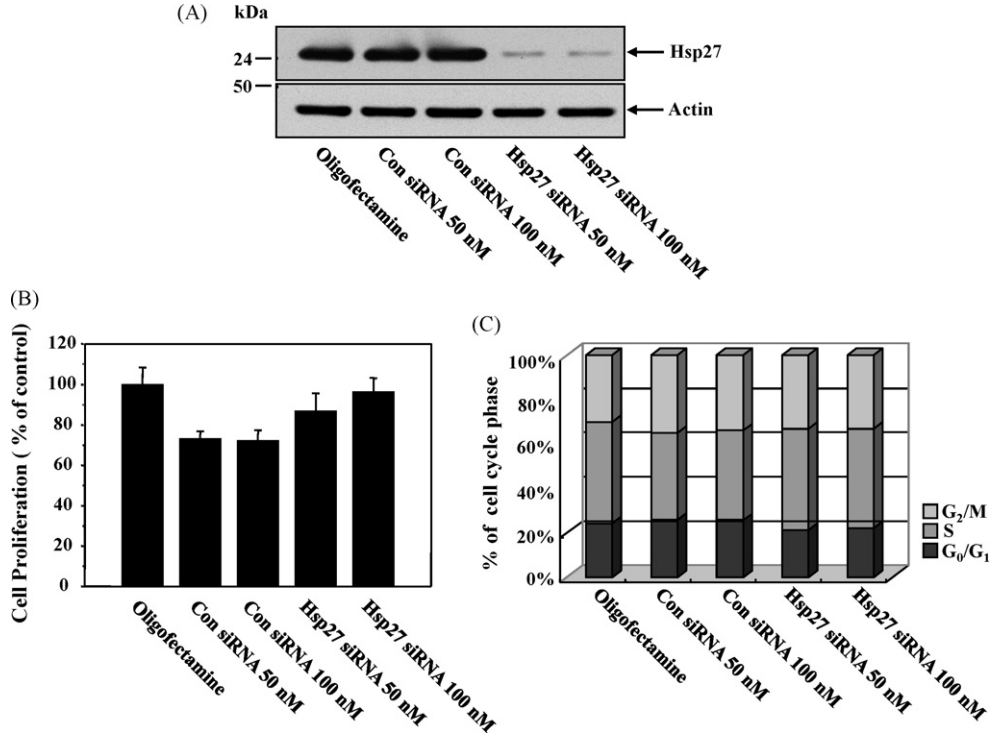

Fig. 2 – Knockdown of the Hsp27 protein does not affect proliferation or cell cycle distribution. (A) HCT-116 cells were transfected with siRNA as described in Section 2, and then lysates were prepared with RIPA buffer. The whole cell lysates (30 μg) were separated using 12.5% SDS-PAGE, and blotted with anti-Hsp27 antibody or anti-actin antibody. (B) Proliferation of transfected HCT-116 cells was determined using the WST-1 assay at 48 h post-treatment. The results were expressed relative to the vehicle-treated cells. (C) HCT-116 cells were transfected with control (Con) siRNA or Hsp27 siRNA for 48 h and harvested, fixed, and stained with propidium iodide. Twenty thousand stained cells were then subjected to FACScalibur analysis. This data is from one of two independent experiments with similar results.

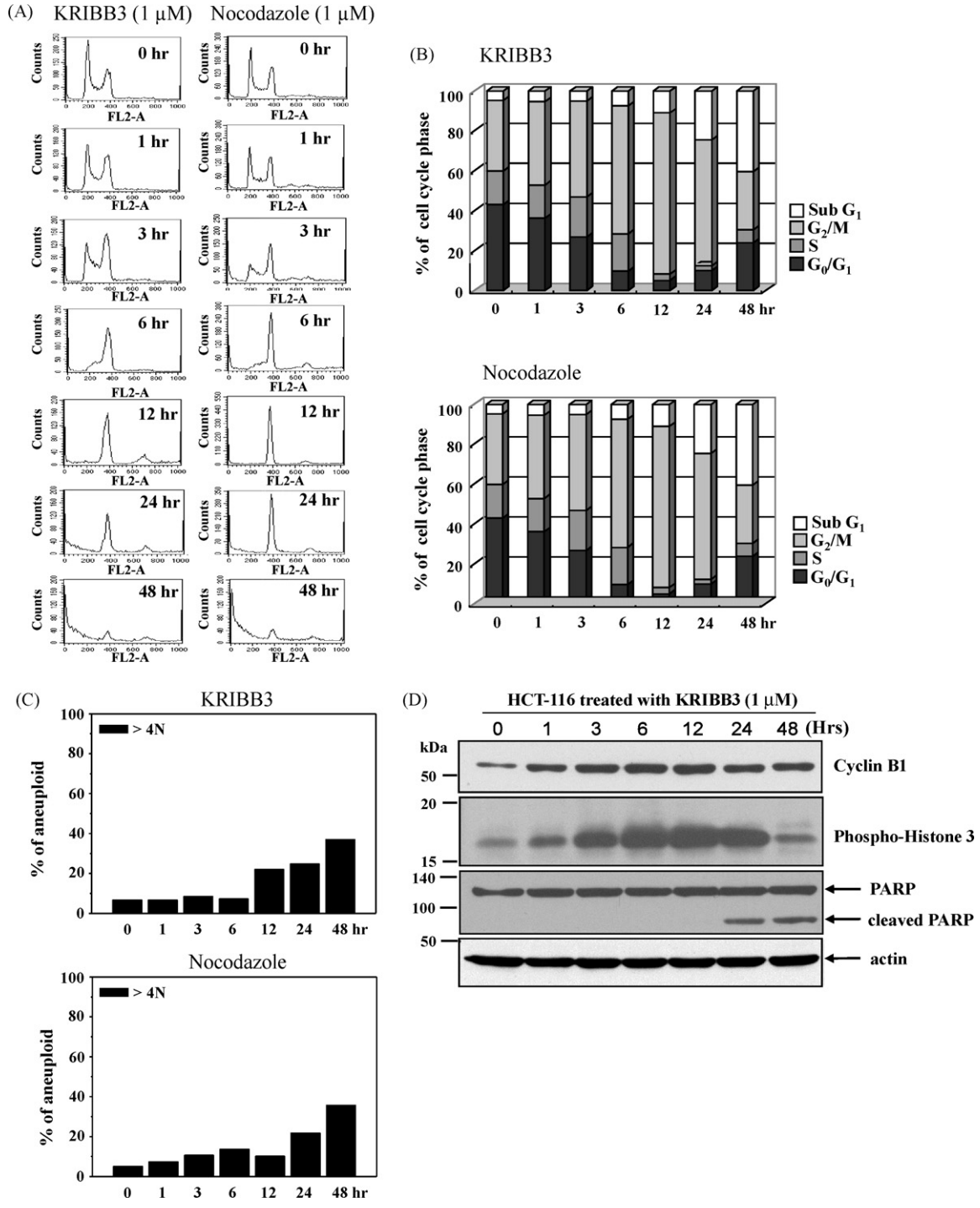

Fig. 3 – KRIBB3 induces cell cycle arrest at the G_2/M phase and causes apoptosis. (A) HCT-116 cells were treated with 1 μM KRIBB3 or nocodazole for 0, 1, 3, 6, 12, 24, or 48 h and harvested, fixed, and stained with propidium iodide. Twenty thousand stained cells were then subjected to FACScalibur analysis. (B) Relative percentages of cells in the sub-G1 (<2 N), G_2/M, S, and G_0/G_1 stages. (C) Relative percentages of hyperploid (>4 N). Populations were derived from the flow cytometric analysis in (A). (D) HCT-116 cells were treated with 1 μM KRIBB3 for different times as indicated, and lysates were prepared with RIPA buffer. Twenty microgram of lysate were resolved by SDS-PAGE and immunoblotted with anti-Cyclin B1, anti-phospho-Histone H3 (Ser 10), anti-PARP, or anti-actin antibody. This data is from one of three independent experiments with similar results.

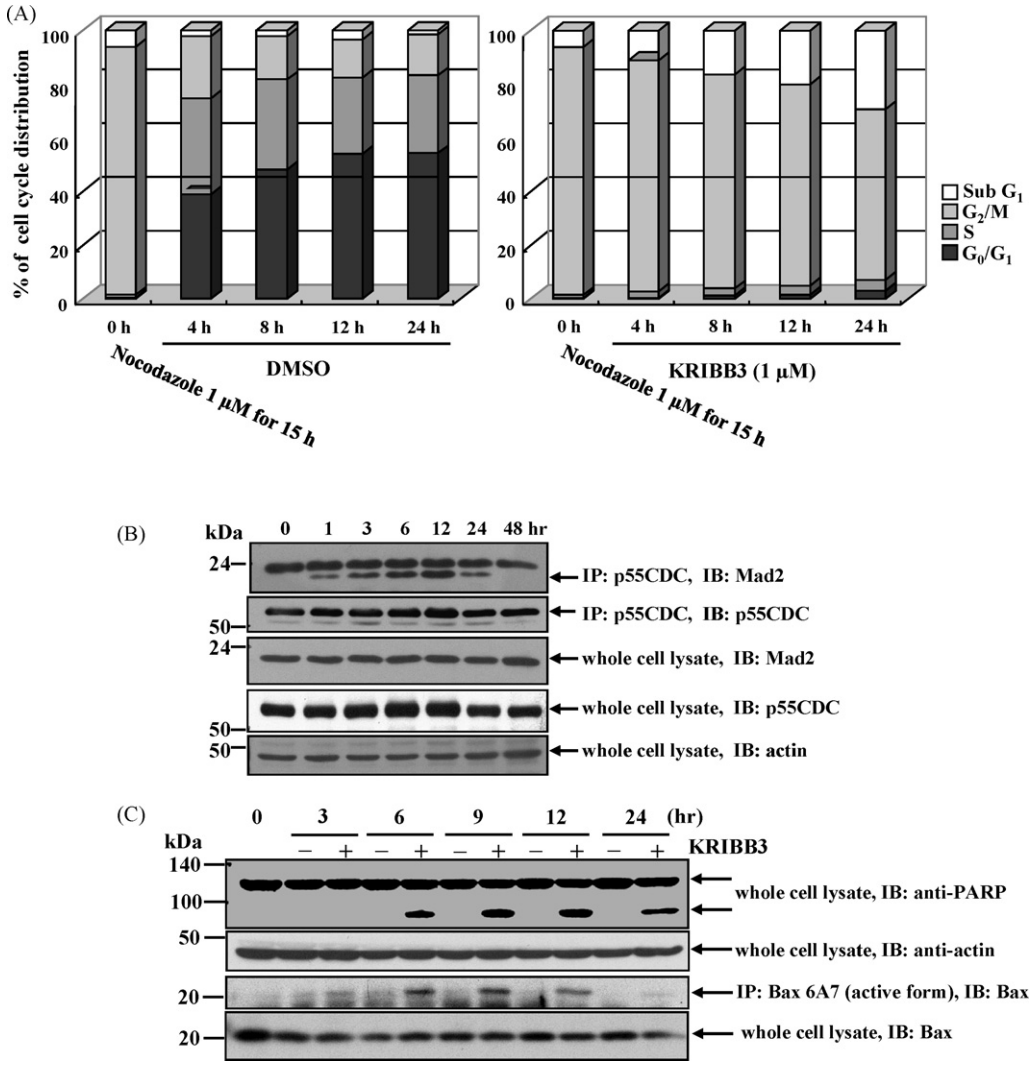

Fig. 4 – KRIBB3 arrests the cell cycle at the mitotic phase through formation of the inhibitory complex Mad2/p55CDC, and induces apoptosis via Bax activation. (A) HCT-116 cells were treated with 1 μM nocodazole for 15 h in order to synchronize the cells at mitosis, as described in Section 2. The collected mitotic cells were replated in 100 mm culture dishes in medium containing 0.1% Me_2SO (DMSO) or KRIBB3 (1 μM). At the indicated time points after nocodazole release, cells were harvested, fixed, and stained with propidium iodide. Twenty thousand stained cells were then subjected to FACScalibur analysis. (B) HCT-116 cells were treated with 1 μM KRIBB3 and incubated for different times as indicated. Four hundred microgram of lysate was immunoprecipitated (IP) with anti-p55CDC antibody and protein G-agarose beads, and precipitants were resolved by SDS-PAGE after washing three times, and then immunoblotted with anti-Mad2 antibody or anti-p55CDC antibody. The same whole cell lysates (WCL) were resolved by SDS-PAGE and immunoblotted with anti-Mad2 antibody, anti-p55CDC antibody, or anti-actin antibody. (C) HCT-116 cells were treated with 1 μM nocodazole for 15 h. The mitotic cells were replated in 100 mm culture dishes in medium containing 0.1% Me_2SO (DMSO) or KRIBB3 (1 μM). At the indicated time points after nocodazole release, cell lysates were prepared with RIPA buffer or with 1% Chaps lysis buffer for active Bax 6A7 detection. Thirty microgram of lysate was resolved by SDS-PAGE and immunoblotted with anti-PARP antibody or anti-actin antibody. Five hundred microgram of Chaps buffer lysate was immunoprecipitated (IP) with anti-Bax 6A7 monoclonal antibody and protein G-agarose beads, and precipitants were resolved by SDS-PAGE after washing three times with Chaps lysis buffer and immunoblotted with anti-Bax monoclonal antibody. Thirty microgram of lysate was resolved by SDS-PAGE and immunoblotted with anti-Bax antibody. This data is from one of two independent experiments with similar results.

Cells were collected at the time indicated, and the profile of the cell cycle was analyzed by FACS. As shown in Fig. 4A, HCT-116 cells were released from a nocodazole-induced mitotic phase arrest after replating cells in the medium with DMSO. However, addition of KRIBB3 (Fig. 4A) into replating medium did not result in the release of mitotic phase arrested cells. These results suggest that KRIBB3 arrested the cell cycle at the same mitotic phase as nocodazole.

3.4. *Time-dependent effect of KRIBB3 in spindle checkpoint-competent cells*

KRIBB3 arrested the cell cycle at the G_2/M phase (Fig. 3). In addition, Cyclin B1, a substrate of APC/C, accumulated following KRIBB3 treatment. These results imply that APC/C activity could be inhibited by KRIBB3. Therefore, we examined whether KRIBB3 exerts its activity through APC/C inhibition. For this experiment, p55CDC (mammalian homologue of CDC20) was immunoprecipitated with an antibody specific to p55CDC, and immunoblotted with an antibody specific to Mad2 (Fig. 4B). Inhibitory association of p55CDC with Mad2 was induced, and reached its maximum 12 h after KRIBB3 treatment. Next, this inhibitory complex decreased 24 h after KRIBB3 treatment, and disappeared 48 h after treatment. However, expression of Mad2 and p55CDC remained unaltered by KRIBB3 treatment. These results suggest that KRIBB3 caused cell cycle arrest at the mitotic phase through the

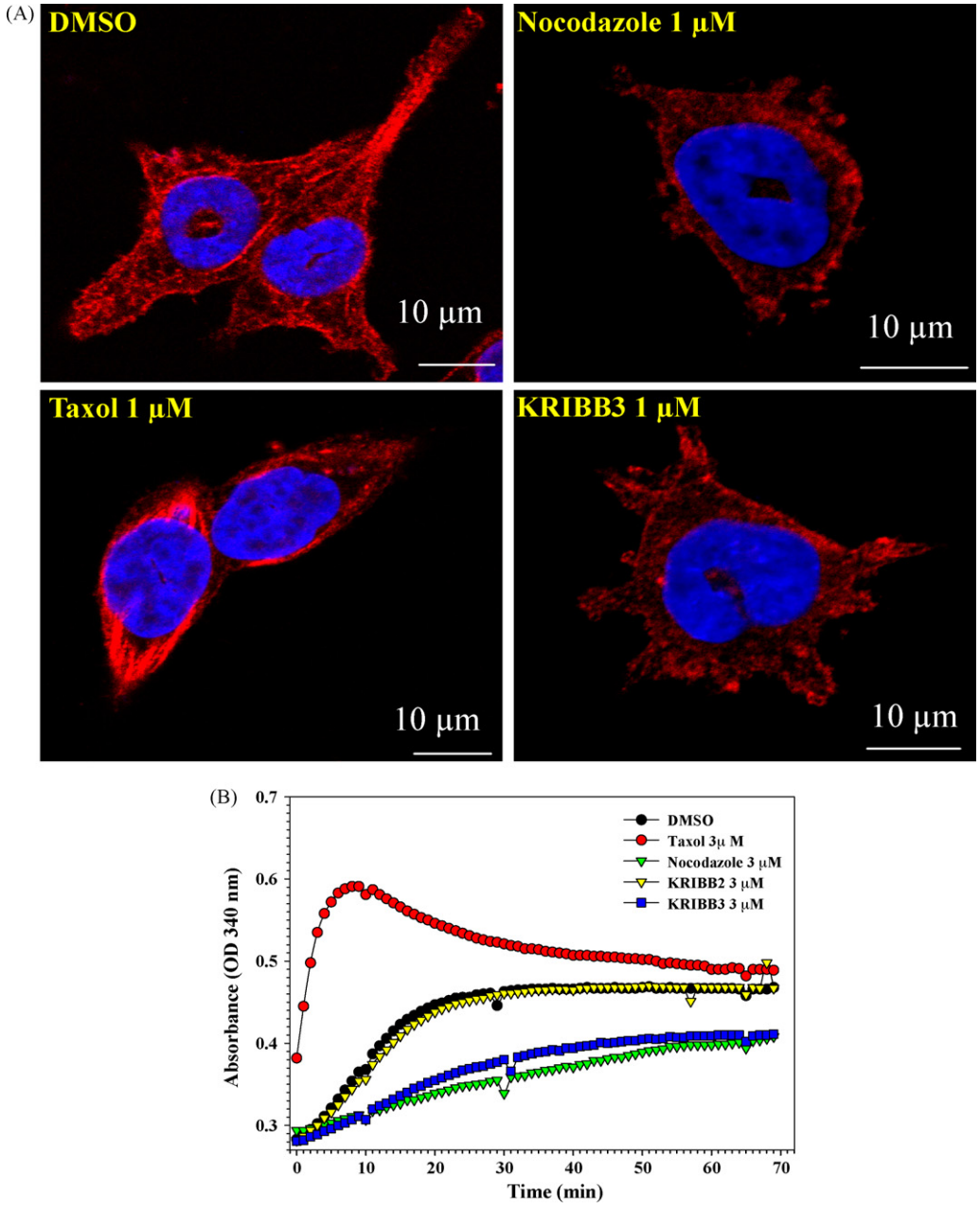

Fig. 5 – Effect of KRIBB3 on the organization of the microtubule cytoskeleton *in vivo* and *in vitro*. (A) HCT-116 cells were incubated with 0.1% Me_2SO, 1 μM nocodazole, 1 μM taxol, or 1 μM KRIBB3 for 6 h. The cellular microtubule network was analyzed by a Carl Zeiss confocal system using monoclonal anti-α-tubulin antibody, fluorescein Texas Red-conjugated goat anti-mouse antibody, and 4,6-diamidino-2-phenylindole. Scale bar, 10 μm. (B) This assay was done using purified tubulins *in vitro*. The tubulins were incubated at 37 °C in the presence of vehicle (Me_2SO), 3 μM taxol, 3 μM nocodazole, 3 μM KRIBB2, or 3 μM KRIBB3, and microtubule formation was measured by the spectrophotometer. This data is from one of two independent experiments with similar results.

formation of the inhibitory checkpoint complex of Mad2/p55CDC. Furthermore, this is consistent with the observation that a decrease of the inhibitory complex resulted in a slippage of the mitotic arrest 48 h after KRIBB3 treatment.

3.5. Induction of apoptosis by KRIBB3 is coupled with Bax activation

The majority of cells were arrested at the G_2/M phase 12 h after KRIBB3 treatment. However, apoptosis was detected 24 h after treatment (Fig. 3). These results imply that slippage of the cell cycle after arrest at the mitotic phase could be important in the induction of apoptosis. Therefore, we collected synchronized mitotic cells and analyzed their cellular response for apoptosis in the presence or absence of KRIBB3. As shown in Fig. 4C, PARP cleavage was detected only from KRIBB3-treated cells.

Bax is a proapoptotic protein of the Bcl-2 family. Under normal conditions, Bax is primarily located in the cytosol as an inactive monomer. Bax is activated upon stimulation by death signals, resulting in a conformational change that targets it to the outer membrane of the mitochondria. In order to test whether Bax activation is involved in KRIBB3-induced apoptosis, cells were treated with KRIBB3 and collected at the indicated time, and lysates were prepared with Chaps lysis buffer. Bax activation was monitored by an immunoprecipitation-coupled Western blot analysis. The monoclonal antibody Bax 6A7 can specifically precipitate the active conformers of Bax [30,31]. Fig. 4C shows that activation of Bax was detected only in lysates prepared from cells treated with KRIBB3. In addition, the temporal pattern of Bax activation is very similar to that of PARP cleavage. These results support the hypothesis that KRIBB3 induces apoptosis through activation of Bax.

3.6. KRIBB3 inhibits microtubule polymerization in vivo and in vitro

It has been very well documented that microtubule inhibitors, including nocodazole, arrest cells at the G_2/M phase and induce apoptosis. In addition, microtubules play crucial roles in maintaining cell morphology and shape. Interestingly, when cells were treated with KRIBB3, cells became round, arrested the cell cycle at the G_2/M phase and underwent apoptosis. In light of these observations, we speculated that microtubules and/or their function could be a potential target of KRIBB3. Therefore, immunofluorescence confocal microscopy was used to examine the effect of KRIBB3 on the microtubule cytoskeleton. The normal distribution of microtubules in untreated HCT-116 cells is shown in Fig. 5A. Paclitaxel treatment resulted in maintenance of microtubule polymerization with an increase in the density of microtubules. In contrast, treatment with KRIBB3 resulted in inhibition of microtubule polymerization and the appearance of short microtubule fragments in the cytoplasm. Similarly, treatment with nocodazole resulted in a diffuse stain visible throughout the cytoplasm, similar to staining for KRIBB3-induced microtubule changes.

Because KRIBB3 disrupted the microtubule organization *in vivo*, we further tested whether KRIBB3 directly inhibits tubulin polymerization *in vitro*. As shown in Fig. 5B, purified tubulins were polymerized to steady state in the presence of GTP at 37 °C in a control sample. As expected, treatment with KRIBB3 inhibited tubulin polymerization compared with DMSO. However, KRIBB2, an inactive structural analogue compound, did not inhibit tubulin polymerization. This result supports a structurally specific activity of KRIBB3 in microtubule polymerization. In the presence of paclitaxel or nocodazole as a positive or a negative control, tubulin polymerization was enhanced or inhibited, respectively.

3.7. KRIBB3 inhibits growth of HCT-116 colon cancer cells in BALB/c nude mice

A HCT-116 tumor xenograft model of nude mice was used to investigate the inhibitory activity of KRIBB3 on tumor growth. HCT-116 cells were implanted subcutaneously into the right flank of nude mice on day 0, and the compound was

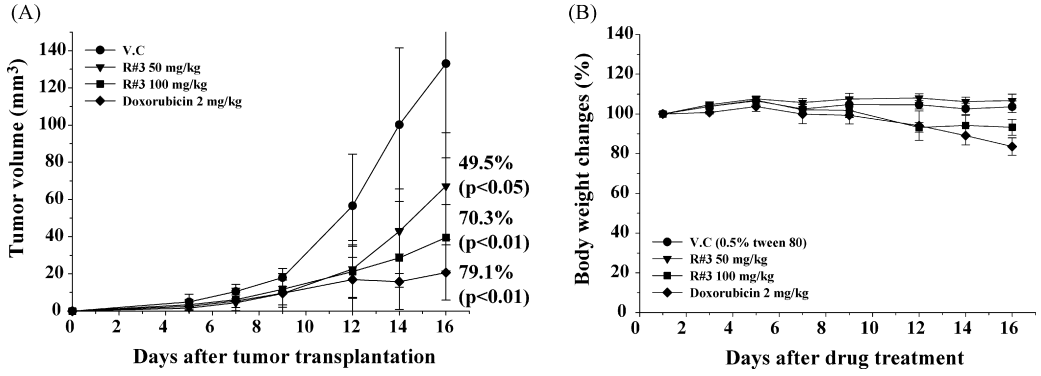

Fig. 6 – KRIBB3 inhibits the growth of HCT-116 colon cancers in nude mice. (A) For the evaluation of the *in vivo* anti-tumor activity of KRIBB3, HCT-116 cells (0.3 ml of 3×10^6 cells/ml) were implanted subcutaneously into the right flank of nude mice on day 0. Compounds were dissolved in 0.5% Tween 80 and were administered intraperitoneally daily for 16 days at a concentration of 50 or 100 mg/kg for KRIBB3 or 2 mg/kg for doxorubicin. The dosage was 0.2 ml per 20 g body weight. These results were obtained from one assay using 24 mice (6 mice for each compound). Tumor volumes were estimated by the formula length (mm) × width (mm) × height (mm)/2, and the results were expressed relative value to the vehicle-treated mice. (B) Body weight was measured on each indicated day using a balance.

administered intraperitoneally daily from day 1 at a concentration of 50 or 100 mg/kg for KRIBB3 or 2 mg/kg for doxorubicin per day. To determine the toxicity of the compound, the body weight of the tumor-bearing animals was measured. On day 16, the mice were sacrificed and the tumors were removed and weighed. Sixteen days after implantation, tumor volume had decreased by 49.5% (50 mg/kg) and 70.3% (100 mg/kg) in mice treated with KRIBB3 compared to control mice (Fig. 6). There was no change in body weight when KRIBB3 was used at 50 mg/kg. However, when KRIBB3 was used at 100 mg/kg, there was a 10.3% loss of body weight. Similarly, when doxorubicin was used as a positive control at 2 mg/kg, a 20% loss of body weight was observed.

4. Discussion

An unexpected finding of this study is that KRIBB3 inhibits tumor cell growth. KRIBB3 was initially discovered from chemical screens to identify inhibitors of migration (but not proliferation) of MDA-MB-231 breast cancer cells [20]. However, it inhibited proliferation of a variety of other malignancies at sub-μM concentration, except MDA-MB-231 and HT-29 (Table 1). KRIBB3 inhibits tumor cell migration and invasion by blocking PKC-dependent phosphorylation of Hsp27 through its direct binding to Hsp27 [20].

Initially, we believed that KRIBB3 blocked cancer cell growth through inhibition of Hsp27. In order to test this possibility, we used Hsp27 siRNA to silence Hsp27 expression and examined its effect on cell proliferation (Fig. 2). Surprisingly, knockdown of Hsp27 did not inhibit proliferation of HCT-116. Therefore, we concluded that the effect of KRIBB3 on proliferation and cell cycle progression was not through Hsp27, but rather through another as yet unidentified KRIBB3 target.

In order to determine the molecular mechanism of KRIBB3-dependent growth inhibition, we analyzed cell cycle progression in a time-dependent manner. Seventy percent of cells were arrested at the G_2/M phase 12 h after KRIBB3 treatment (Fig. 3A and B). Cell cycle arrest at the G_2/M phase was further confirmed by detecting the G_2/M phase-specific protein Cyclin B1 and phosphorylation of Histone H3 (Ser 10) (Fig. 3D). There are many possible KRIBB3 targets responsible for a KRIBB3-dependent G_2/M phase arrest. Accumulation of Cyclin B1 implies that its degradation pathway could be blocked by KRIBB3. Cyclin B1 is degraded by the proteasome in a cell cycle dependent manner after APC/C-dependent-ubiquitination.

Therefore, we decided to test whether KRIBB3 inhibits APC/C-dependent activity. APC/C-dependent-ubiquitination is dependent on CDC20 (p55CDC, mammalian homologue) to recognize its substrate. This substrate recognition protein is associated with its inhibitory protein Mad2. Therefore, we examined the formation of the inhibitory complex p55CDC/Mad2 in a time-dependent manner after KRIBB3 treatment (Fig. 4B). As expected, KRIBB3 treatment induced association of p55CDC with the inhibitory protein Mad2. This inhibitory complex may block APC/C-dependent Cyclin B1 degradation.

This leads to the question of how KRIBB3 induces the inhibitory complex of p55CDC/Mad2. Because microtubule poisons such as vinca alkaloids cause all kinetochores to become unattached, thereby generating a mitotic-checkpoint signal, we decided to test whether KRIBB3 could inhibit microtubule structure. We carried out indirect immunofluorescence microscopy to check the microtubule cytoskeleton *in vivo*. Cells treated with KRIBB3 showed short microtubule fragments in the cytoplasm (Fig. 5A). This structure is similar to microtubules in cells treated with nocodazole. Furthermore, *in vitro*, purified tubulin polymerization was inhibited in the presence of KRIBB3 or nocodazole, and enhanced in the presence of paclitaxel (Fig. 5B). From this, we concluded that KRIBB3 inhibited tubulin polymerization. The inhibitory activity of KRIBB3 on tubulin polymerization is similar to that of nocodazole. However, KRIBB2, an inactive structural analogue of KRIBB3, did not show any inhibitory effect on tubulin polymerization (Fig. 5B). Consistent with this, KRIBB2 did not inhibit proliferation of HCT-116 cells (Fig. 1). These results support our conclusion that inhibition of tubulin polymerization by KRIBB3 caused mitotic phase arrest and growth inhibition.

Because p53 has been shown to be involved in apoptosis and more than 50% of human cancers have mutated p53, it is important for drugs to be able to induce apoptosis in a p53-independent manner. Therefore, we tested whether KRIBB3 could inhibit the growth of p53 null cancer cell lines. Fortunately, KRIBB3 was able to induce cell cycle arrest at the mitotic phase, and apoptosis of both HCT-116 (p53+/+) and DU-145 (p53−/−) cells. This suggests that induction of apoptosis following slippage of the mitotic checkpoint may not depend on the p53-mediated tetraploid checkpoint.

Among 12 cancer cell lines, only MDA-MB-231 and HT-29 were relatively resistant to KRIBB3-induced growth inhibition (Table 1). Currently, we do not know why these cells are refractory to KRIBB3. Recently, Tao et al. reported that cells that can sustain a long-term (48 h) arrest in mitosis (e.g., HT-29 colorectal adenocarcinoma cells) are less susceptible to taxol-mediated killing than cells that more rapidly adapt into G1 after less than 24 h of drug exposure (e.g., HCT-116 colorectal carcinoma cells) [31]. Therefore, it is likely that difference(s) in checkpoint response determine the sensitivity to inhibitors of microtubule dynamics.

Normal cells have a robust mitotic checkpoint in which one unattached kinetochore can generate a signal strong enough to inhibit all cellular APC/C activity and therefore block progress to anaphase. However, when checkpoint components are mutated or their expression is low, they cannot produce strong enough signals to arrest the cell cycle. When HCT-116 cells were treated with 1 μM KRIBB3 for 48 h, 43% of the cells were in the sub-G1 phase, indicating apoptosis (Fig. 3). However, when Human Foreskin Fibroblast (HFF) cells (normal cell line) were treated with 1 μM KRIBB3 for 48 h, only 10% of cells were sub-G1 phase (data not shown). This result supports the hypothesis that HCT-116 cells are more sensitive to KRIBB3 than HFF cells. In addition, many cancer cells divide *in vivo* more frequently than normal cells, and therefore frequently pass through a stage of vulnerability to mitotic poisons. Therefore, cancer cells may be relatively sensitive to KRIBB3 compared with normal cells.

Failure in cancer chemotherapy is often related to multi-drug resistance (MDR). Many microtubule-interacting drugs

such as the taxanes and vinblastine, are well-known substrates of P-glycoprotein (MDR1). This means that tumor cells can easily acquire drug resistance by overexpressing the MDR1 pump. The development of new compounds that are effective against drug-resistant cells is therefore important for cancer therapy. These results show that KRIBB3 exhibits a similar potency regardless of P-glycoprotein status (HCT-15 vs. HCT-116), indicating that KRIBB3 is not a substrate of P-glycoprotein, thereby suggesting that KRIBB3 is superior to other antimitotic agents in this regard.

This study reports the biological properties of the low-molecular-weight compound KRIBB3, which displays strong antimitotic activity against cancer cells. *In vitro*, KRIBB3 exerts significant antitumoral activity against a variety of malignancies (colon, prostate, breast, and lung). The mode of action of KRIBB3 as a tubulin inhibitor was shown by an *in vitro* tubulin polymerization assay and indirect immunofluorescence microscopy. The KRIBB3 selectively arrested cell cycle progression at the mitotic phase by activating the mitotic spindle checkpoint. When KRIBB3 was administered, tumor volume decreased by 49.5% (50 mg/kg) and 70.3% (100 mg/kg) compared to control mice. The unique structural and biological properties of KRIBB3 make it an attractive candidate for further development toward potential clinical applications.

Acknowledgments

Grant support: KRIBB Research Initiative Program, the National Chemical Genomics Research Program, and Center for Biological Modulators of the 21st Century Frontier Research Program.

REFERENCES

[1] Zhou J, Giannakakou P. Targeting microtubules for cancer chemotherapy. Curr Med Chem Anticancer Agents 2005;5:65–71.
[2] Jordan MA, Wilson L. Microtubules as a target for anticancer drugs. Nat Rev Cancer 2004;4:253–65.
[3] Mollinedo F, Gajate C. Microtubules, microtubule-interfering agents and apoptosis. Apoptosis 2003;8: 413–50.
[4] Weaver BA, Cleveland DW. Decoding the links between mitosis, cancer, and chemotherapy: the mitotic checkpoint, adaptation, and cell death. Cancer Cell 2005;8:7–12.
[5] Bharadwaj R, Yu H. The spindle checkpoint, aneuploidy, and cancer. Oncogene 2004;23:2016–27.
[6] Sudakin V, Chan GK, Yen TJ. Checkpoint inhibition of the APC/C in HeLa cells is mediated by a complex of BUBR1, BUB3, CDC20, and MAD2. J Cell Biol 2001;154:925–36.
[7] Tang Z, Bharadwaj R, Li B, Yu H. Mad2-Independent inhibition of APCCdc20 by the mitotic checkpoint protein BubR1. Dev Cell 2001;1:227–37.
[8] Raff MC. Social controls on cell survival and cell death. Nature 1992;356:397–400.
[9] Tang C, Willingham MC, Reed JC, Miyashita T, Ray S, Ponnathpur V, et al. High levels of p26BCL-2 oncoprotein retard taxol-induced apoptosis in human pre-B leukemia cells. Leukemia 1994;8:1960–9.
[10] Gajate C, Barasoain I, Andreu JM, Mollinedo F. Induction of apoptosis in leukemic cells by the reversible microtubule-disrupting agent 2-methoxy-5-(2′,3′,4′-trimethoxyphenyl)-2,4,6-cycloheptatrien-1 -one: protection by Bcl-2 and Bcl-X(L) and cell cycle arrest. Cancer Res 2000;60:2651–9.
[11] Puthalakath H, Huang DC, O'Reilly LA, King SM, Strasser A. The proapoptotic activity of the Bcl-2 family member Bim is regulated by interaction with the dynein motor complex. Mol Cell 1999;3:287–96.
[12] Puthalakath H, Villunger A, O'Reilly LA, Beaumont JG, Coultas L, Cheney RE, et al. Bmf: a proapoptotic BH3-only protein regulated by interaction with the myosin V actin motor complex, activated by anoikis. Science 2001;293:1829–32.
[13] Marani M, Tenev T, Hancock D, Downward J, Lemoine NR. Identification of novel isoforms of the BH3 domain protein Bim which directly activate Bax to trigger apoptosis. Mol Cell Biol 2002;22:3577–89.
[14] Jordan MA, Thrower D, Wilson L. Mechanism of inhibition of cell proliferation by Vinca alkaloids. Cancer Res 1991;51:2212–22.
[15] Schiff PB, Fant J, Horwitz SB. Promotion of microtubule assembly in vitro by taxol. Nature 1979;277:665–7.
[16] Manfredi JJ, Horwitz SB. Taxol: an antimitotic agent with a new mechanism of action. Pharmacol Ther 1984;25:83–125.
[17] Dumontet C, Sikic BI. Mechanisms of action of and resistance to antitubulin agents: microtubule dynamics, drug transport, and cell death. J Clin Oncol 1999;17:1061–70.
[18] Fardel O, Lecureur V, Guillouzo A. The P-glycoprotein multidrug transporter. Gen Pharmacol 1996;27:1283–91.
[19] Cole SP, Deeley RG. Multidrug resistance mediated by the ATP-binding cassette transporter protein MRP. Bioessays 1998;20:931–40.
[20] Shin KD, Lee MY, Shin DS, Lee S, Son KH, Koh S, et al. Blocking tumor cell migration and invasion with biphenyl isoxazole derivative KRIBB3, a synthetic molecule that inhibits Hsp27 phosphorylation. J Biol Chem 2005;280:41439–48.
[21] Blackburn RV, Galoforo SS, Berns CM, Armour EP, McEachern D, Corry PM, et al. Comparison of tumor growth between hsp25- and hsp27-transfected murine L929 cells in nude mice. Int J Cancer 1997;72:871–7.
[22] Katoh M, Koninkx J, Schumacher U. Heat shock protein expression in human tumours grown in severe combined immunodeficient mice. Cancer Lett 2000;161:113–20.
[23] Love S, King RJ. A 27 kDa heat shock protein that has anomalous prognostic powers in early and advanced breast cancer. Br J Cancer 1994;69:743–8.
[24] Oesterreich S, Weng CN, Qiu M, Hilsenbeck SG, Osborne CK, Fuqua SA. The small heat shock protein hsp27 is correlated with growth and drug resistance in human breast cancer cell lines. Cancer Res 1993;53:4443–8.
[25] Cornford PA, Dodson AR, Parsons KF, Desmond AD, Woolfenden A, Fordham M, et al. Heat shock protein expression independently predicts clinical outcome in prostate cancer. Cancer Res 2000;60:7099–105.
[26] Ehrenfried JA, Herron BE, Townsend Jr CM, Evers BM. Heat shock proteins are differentially expressed in human gastrointestinal cancers. Surg Oncol 1995;4:197–203.
[27] Langdon SP, Rabiasz GJ, Hirst GL, King RJ, Hawkins RA, Smyth JF, et al. Expression of the heat shock protein HSP27 in human ovarian cancer. Clin Cancer Res 1995;1:1603–9.
[28] Arts HJ, Hollema H, Lemstra W, Willemse PH, De Vries EG, Kampinga HH, et al. Heat-shock-protein-27 (hsp27) expression in ovarian carcinoma: relation in response to chemotherapy and prognosis. Int J Cancer 1999;84:234–8.
[29] Han DC, Lee MY, Shin KD, Jeon SB, Kim JM, Son KH, et al. 2′-Benzoyloxycinnamaldehyde induces apoptosis in human

carcinoma via reactive oxygen species. J Biol Chem 2004;279:6911–20.
[30] Hsu YT, Youle RJ. Bax in murine thymus is a soluble monomeric protein that displays differential detergent-induced conformations. J Biol Chem 1998;273:10777–83.
[31] Tao W, South VJ, Zhang Y, Davide JP, Farrell L, Kohl NE, et al. Induction of apoptosis by an inhibitor of the mitotic kinesin KSP requires both activation of the spindle assembly checkpoint and mitotic slippage. Cancer Cell 2005;8:49–59.